Effects of Mutations in Aspartate 14 on the Spectroscopic Properties of the $[Fe_3S_4]^{+,0}$ Clusters in *Pyrococcus furiosus* Ferredoxin†

Randall E. Duderstadt, Christopher R. Staples, Phillip S. Brereton, Michael W. W. Adams, and Michael K. Johnson*

Departments of Chemistry and Biochemistry & Molecular Biology and Center for Metalloenzyme Studies, University of Georgia, Athens, Georgia 30602

Received March 23, 1999; Revised Manuscript Received June 2, 1999

ABSTRACT: The properties of $[Fe_3S_4]^{+,0}$ clusters in wild-type and mutant forms of Pf Fd with Asp, Ser, Cys, Val, His, Asn, and Tyr residues occupying position 14, i.e., proximal to the three μ_2-S atoms of the cluster, have been investigated by the combination of EPR, variable-temperature magnetic circular dichroism (VTMCD), and resonance Raman (RR) spectroscopies. Two distinct types of $[Fe_3S_4]$ clusters are identified on the basis of the breadth of the $S = {}^1/_2$ $[Fe_3S_4]^+$ EPR resonances and the marked differences in the VTMCD spectra of the $S = 2$ $[Fe_3S_4]^0$ clusters. On the basis of the available NMR data for $[Fe_3S_4]^{+,0}$ clusters in ferredoxins, the distinctive properties of these two types of $[Fe_3S_4]$ clusters are interpreted in terms of different locations of the more strongly coupled pair of irons in the oxidized clusters and the valence-delocalized pair in the reduced clusters. Near-IR VTMCD measurements indicate the presence of $S = {}^9/_2$ valence-delocalized pairs in both types of $[Fe_3S_4]^0$ clusters, and the spin-dependent delocalization energies associated with the Fe−Fe interactions were determined to be ∼4300 cm^{-1} in both cases. We conclude that the nature of the residue at position 14 in *Pyrococcus furiosus* ferredoxin is an important determinant of the location of the reducible pair of irons in a $[Fe_3S_4]^{+,0}$ cluster, and the redox properties of the wild-type and mutant ferredoxins are discussed in light of these new results.

Since their discovery in 1980 (*1*), iron−sulfur clusters containing cubane-type $[Fe_3S_4]^{+,0}$ cores have emerged as intrinsic redox components of proteins in Eucarya, Bacteria, and Archaea. They occur indigenously in several mono- and dicluster ferredoxins (Fds) as well as in succinate dehydrogenase, fumarate reductase, glutamate synthase, NiFe hydrogenase, and nitrate reductase and have been the subject of a recent review (*2*). However, in many Fe−S proteins, $[Fe_3S_4]^+$ clusters have been shown to be the initial products of oxidative degradation of $[Fe_4S_4]$ clusters (*3*), and both types of cluster are frequently ligated by similar arrangements of cysteine residues (*4*). For $[Fe_4S_4]$ clusters, the first three cysteines commonly occur in a C-X-X-C-X-X-C arrangement (positions I−III) with the fourth being more remote and occurring in a C-P arrangement (position IV). Indigenous $[Fe_3S_4]$ clusters frequently have a noncoordinating residue such as V, L, A, or I in place of C at position II, and it is the Fe ligated by the residue occupying position II that is lost in oxidative $[Fe_4S_4] \rightarrow [Fe_3S_4]$ cluster conversions. Consequently, sequence and/or structural data or alternatively in vivo spectroscopic studies are essential for demonstrating that $[Fe_3S_4]$ clusters are not artifacts of aerobic isolation or chemical oxidation. X-ray crystal structures have been reported for six proteins containing oxidized $[Fe_3S_4]^+$ cores [*Azotobacter vinelandii* FdI (*5*−*7*), *Desulfovibrio gigas* FdII (*8*, *9*), aconitase (*10*, *11*), NiFe hydrogenases from *D. gigas* (*12*) and *Desulfovibrio vulgaris* Miyazaki (*13*), and *Sulfolobus* sp. strain 7 Fd (*14*)] and for one protein [*A. vinelandii* FdI (*15*)] and one model complex (*16*) containing reduced $[Fe_3S_4]^0$ cores. In both oxidation states, the structure is best described as a cubane-type $[Fe_4S_4]$ cluster minus one of the Fe atoms.

The available evidence indicates that cuboidal $[Fe_3S_4]^{+,0}$ clusters function exclusively in an electron transfer or redox sensing role under physiological conditions and exhibit midpoint potentials for the one-electron redox couple in the range of 90 to −460 mV (*2*). The $S = {}^1/_2$ ground state of the oxidized $[Fe_3S_4]^+$ cluster and the $S = 2$ ground state of the reduced $[Fe_3S_4]^0$ cluster have both been rationalized on the basis of the spin coupling models and valence delocalization schemes originally developed by Münck and coworkers (*17*−*19*). In the oxidized state, a simple Heisenberg−Dirac−van Vleck (HDvV) exchange Hamiltonian of the form $H = J_{12}S_1S_2 + J_{23}S_2S_3 + J_{13}S_1S_3$ involving three high-spin Fe^{3+} ions ($S_1 = S_2 = S_3 = {}^5/_2$) predicts an $S = {}^1/_2$ ground state provided all the coupling constants are greater than zero ($J_{ij} > 0$), i.e., antiferromagnetic interaction, with J_{13}/J_{23} between 0.5 and 1, J_{12}/J_{23} between 0.6 and 1, and $|J_{12} - J_{13}|/J_{12}$ of <0.2, i.e., asymmetric coupling with $J_{12} \approx J_{13} < J_{23}$, but with comparable values for all three coupling constants. Such a model predicts that the first excited state will also have $S = {}^1/_2$ provided that J_{12}/J_{23} is between 0.8 and 1, with the ground state corresponding to the more strongly coupled pair having $S_{23} = 2$ ($S_{23} = S_2 + S_3$) and

† This work was supported by a grant from the NIH (GM45597 to M.W.W.A. and M.K.J.) and a NSF Research Training Group Award to the Center for Metalloenzyme Studies (DBI-9413236).

* To whom correspondence should be addressed: Department of Chemistry, University of Georgia, Athens, GA 30602. Telephone: (706) 542-9378. Fax: (706) 542-2353. E-mail: johnson@sunchem.chem.uga.edu.

10.1021/bi990670l CCC: $18.00
Published on Web 07/14/1999

the first excited state corresponding to $S_{23} = 3$. Population of the low-lying $S = {}^1/_2$ excited state has been invoked to explain the EPR relaxation properties and the anomalous temperature dependence of the EPR line shape exhibited by $[Fe_3S_4]^+$ clusters in some bacterial Fds, e.g., *D. gigas* FdII (*20*). However, this analysis leads to an estimate of J of around 40 cm^{-1}, which is much lower than the lower limit of 200 cm^{-1} for J determined in subsequent saturation magnetization studies with oxidized *D. gigas* FdII (*21*) and the value estimated on the basis of NMR studies of the β-CH_2 cysteinate protons of the $[Fe_3S_4]^+$ cluster in the same protein ($J = 300$ cm^{-1}; *22*). Strong support for the values based on the saturation magnetization and NMR analyses comes from the recent determination of the exchange coupling constant of an $Fe^{3+}-Fe^{3+}$ pair in a cubane-type $[Fe_4S_4]$ cluster ($J \approx 300$ cm^{-1}; *23*). NMR is the only technique capable of assigning the cysteines ligating specific Fe atoms, since the asymmetric coupling of the three Fe^{3+} ions results in different temperature dependencies for the contact shifts of coordinating cysteine protons. This approach has thus far been applied to three monocluster 3Fe Fds, and two distinct types of sequence specific assignments have been observed. The unique Fe site in the above scheme (S_1) was found to be ligated by CysI in *Pyrococcus furiosus* Fd (*24*) which has Asp in place of CysII, and by CysIV in *D. gigas* FdII (*22*) and *Thermococcus litoralis* Fd (*25*) which both have Cys at position II.

For reduced $[Fe_3S_4]^0$ clusters, Mössbauer studies revealed that the additional electron is equally shared by two Fe sites, resulting in a valence-delocalized pair $[Fe^{2.5+}Fe^{2.5+}]$ and a high-spin Fe^{3+} site (*1*, *19*, *26*). The $S = 2$ ground state, identified initially via variable-temperature magnetic circular dichroism (VTMCD) studies (*27*), was rationalized in terms of antiferromagnetic exchange interaction between an $S = {}^9/_2$ valence-delocalized pair and the $S = {}^5/_2$ high-spin Fe^{3+} site (*19*). Spin-dependent delocalization (SDD) (also known as double exchange) in addition to the conventional HDvV exchange interaction was introduced to explain the electron delocalization and the ferromagnetic nature of the interaction within the valence-delocalized pair (*19*, *28*). The interplay of double exchange, HDvV exchange, and vibronic trapping has since proven to be essential for understanding intracluster spin coupling and valence delocalization in Fe−S clusters in general (*29*, *30*). However, direct measurement of the spin-dependent resonance delocalization energy has recently been possible (*31*), as a result of the discovery of valence-delocalized $S = {}^9/_2$ $[Fe_2S_2]^+$ clusters in mutant forms of *Clostridium pasteurianum* 2Fe Fd (*32*, *33*). The recent success of Holm and co-workers in preparing and characterizing synthetic clusters with a cuboidal $[Fe_3S_4]^0$ core has demonstrated unequivocally that the valence delocalization scheme and $S = 2$ ground state is an intrinsic property of a $[Fe_3S_4]^0$ cluster as opposed to being a consequence of the protein environment (*16*). Unfortunately, it has not yet been possible to identify NMR resonances from the β-CH_2 protons and thereby provide sequence specific assignments of the cysteines ligating the valence-delocalized and valence-localized Fe sites of a protein-bound $[Fe_3S_4]^0$ center via temperature dependence studies (*34*).

In this work, we report on spectroscopic characterization of the $[Fe_3S_4]^{+,0}$ clusters in mutant forms of the 4Fe Fd ($M_r \sim 7500$) from the hyperthermophilic archaeon *P. furiosus* (*35*), in which Asp14 at position II has been replaced with Cys, Ser, Val, His, Asn, and Tyr (*36*). The combination of EPR, VTMCD, and resonance Raman (RR) spectroscopies is used to show that a $[Fe_3S_4]^{+,0}$ is either assembled in the protein expressed in *Escherichia coli* (D14V, D14H, D14N, and D14Y) or generated from the assembled $[Fe_4S_4]^{2+,+}$ clusters via ferricyanide oxidation (wild type, D14C, and D14S). Near-IR VTMCD studies are shown to be particularly effective for locating and assigning the transitions associated with the $S = {}^9/_2$ valence-delocalized pair of a $[Fe_3S_4]^0$ cluster and thereby providing a direct assessment of the resonance delocalization energy. Analysis of the EPR and VTMCD data for these mutants suggests that these techniques are sensitive to the location of the unique Fe site in oxidized and reduced $[Fe_3S_4]^{+,0}$ clusters, respectively. This leads to the conclusion that the nature of the residue at position II is an important determinant of both the redox properties and the specific pairwise intracluster Fe interactions in $[Fe_3S_4]^{+,0}$ clusters.

EXPERIMENTAL PROCEDURES

Wild-Type and Mutant Forms of P. furiosus Fd. The construction, expression, and purification of the recombinant wild-type (WT) and mutant 3Fe Fd samples used in this work has been described previously (*36*). All samples were in 100 mM Tris-HCl buffer (pH 7.8) unless otherwise stated. The wild type and D14C and D14S mutants were purified anaerobically in the 4Fe form and were treated with a 5-fold (wild type and D14S) or 15-fold (D14C) excess of ferricyanide at room temperature for 15 min to generate the 3Fe forms. Excess oxidant was removed by ultrafiltration, and the resulting sample was washed with 25 mL of 100 mM Tris-HCl buffer (pH 7.8) containing a 15-fold excess of EDTA prior to spectroscopic measurements. Samples were reduced anaerobically using a 10-fold excess of sodium dithionite taken from a freshly prepared stock solution in 100 mM Tris-HCl buffer (pH 7.8). All anaerobic sample handling was carried out in a Vacuum Atmospheres glovebox (<1 ppm O_2) under argon.

Spectroscopic Methods. Room-temperature UV−visible absorption measurements were recorded over a range of 200−800 nm using a Shimadzu UV-3101PC UV−Vis−NIR scanning spectrophotometer. VTMCD spectra were collected for samples containing 50% (v/v) glycerol (native) or 55% (v/v) Aldrich poly(ethylene glycol) using a Jasco J715 (180−1000 nm) or J-730 (700−2000 nm) spectropolarimeter mated to an Oxford Instruments SM-3 (0−5 T) or Spectromag 4000 (0−7 T) split-coil superconducting magnet. Magnetic fields of either 4.5 or 6.0 T were used for the MCD experiments. The MCD intensities are expressed as $\Delta\epsilon$ ($\epsilon_{LCP} - \epsilon_{RCP}$) where ϵ_{LCP} and ϵ_{RCP} are the molar extinction coefficients for the absorption of left and right circularly polarized light, respectively. X-band (~9.5 GHz) EPR spectra were obtained using a Bruker ESP-300E EPR spectrometer equipped with Oxford Instruments ESR-9 flow cryostat.

Resonance Raman spectra were recorded with an Instruments SA U1000 spectrometer fitted with a cooled RCA 31034 photomultiplier tube, using lines from a Coherent Innova 100 10 W Ar^+ laser or a Coherent Innova 200-K2 Kr^+ laser. Scattering was collected at 90° from the surface of a frozen 10 μL droplet of protein solution in a microcup of a gold-plated copper sample holder on the coldfinger of

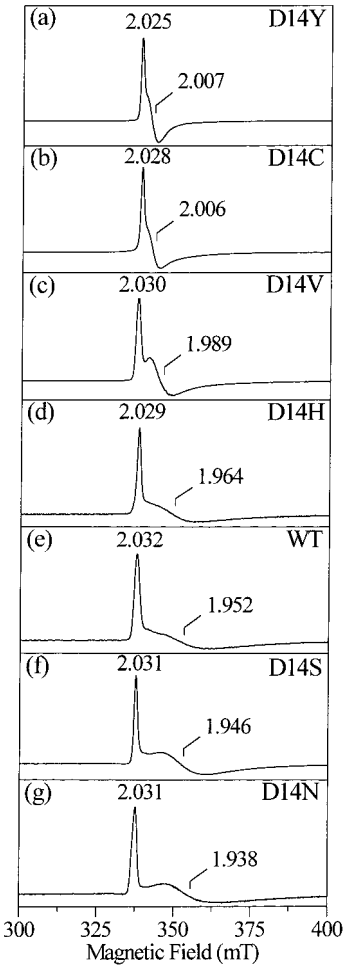

FIGURE 1: X-band EPR spectra of $[Fe_3S_4]^+$ clusters in wild-type and mutant forms of *P. furiosus* Fd. All spectra were recorded at 4.2 K under the following conditions: microwave power, 1 mW; microwave frequency, 9.60 GHz; and modulation amplitude, 0.63 mT. All samples were in 100 mM Tris-HCl buffer (pH 7.8): (a) 178 μM D14Y mutant, (b) 271 μM D14C mutant, (c) 379 μM D14V mutant, (d) 160 μM D14H mutant, (e) 225 μM wild type, (f) 275 μM D14S mutant, and (g) 308 μM D14N mutant. Marked *g*-values correspond to the positive maximum and crossover.

an Air Products Displex model CSA-202E closed cycle refrigerator. Band positions were calibrated using the excitation wavelength, and are accurate to ± 0.5 cm^{-1}. Raman spectra of the same sample obtained at different wavelengths were normalized to the intensity of the ice band at 230 cm^{-1}, which serves as an internal standard. The spectrum of the frozen buffer solution, normalized to the intensity of the ice band at 231 cm^{-1}, and a linear ramp fluorescent background have been subtracted from all the spectra described in this work.

RESULTS AND DISCUSSION

Oxidized [Fe_3S_4]$^+$ Clusters: X-band EPR, VTMCD, and RR (excitation at 457.9 nm) spectra for $[Fe_3S_4]^+$ clusters in *P. furiosus* Fd with Asp, Cys, Ser, Val, His, Asn, and Tyr residues in the pocket proximal to the three μ_2-S atoms (position II) are compared in Figures 1−3, respectively. While relatively minor variations are apparent in the VTMCD and RR spectra, the EPR spectra exhibit marked differences in the line width of the $S = {}^1/_2$ resonance (see Figure 1). Moreover, the range of EPR spectra observed for these mutants mirrors the variability reported for biological $[Fe_3S_4]^+$ clusters in general. All $[Fe_3S_4]^+$ clusters exhibit fast-relaxing resonances centered around $g = 2.01$ in the oxidized protein that are only observed at temperatures below 30 K. However, these resonances can vary significantly in terms of both line shape and apparent *g*-value anisotropy in different proteins (*2*). They invariably exhibit a well-defined low-field *g*-value at $g \sim 2.02$, but frequently have poorly resolved high-field components due to conformational microheterogeneity (*37*), which leads to a distribution in the single Fe^{3+} ion zero-field splitting (*D*) and exchange coupling parameters (*J*) in frozen samples (*38*−*40*). This can be viewed as a type of "*g*-strain" (*41*) that can qualitatively alter the observed spectrum rather than being apparent solely in terms of line width contributions. Hence, the *g*-values obtained for spectral simulations do not necessarily correspond to the principal components of the **g**-tensor.

The EPR line shapes of the *P. furiosus* 3Fe mutants were invariant to microwave power and temperature over the ranges 1−100 mW and 4.2−25 K, respectively, and can be divided into two types. Type 1 corresponds to D14Y, D14C, and D14V and has narrower resonances ($g_{max} \sim 2.03$, $g_{crossover} \sim 2.00$). Type 2 corresponds to the wild type, D14N, D14S, and D14H and has much broader resonances ($g_{max} \sim 2.03$, $g_{crossover} \sim 1.95$), indicative of more severe conformational distribution. Recent analysis of the ^{57}Fe hyperfine coupling constants of the $[Fe_3S_4]^+$ cluster in wild-type *P. furiosus* Fd, as deduced by ^{57}Fe-ENDOR, indicated that the ground state corresponds to the more strongly coupled pair having an S_{23} of 2, as in other Fds (*42*). However, the ground state has more mixing of the low-lying $S = {}^1/_2$ state with an S_{23} of 3 than other 3Fe Fds, as a result of less symmetrical coupling, and this presumably accounts for the extremely broad *g* distribution associated with this conformation. Thus far, sequence specific NMR assignments are only available for the oxidized $[Fe_3S_4]^+$ clusters in *P. furiosus* Fd (Asp at position II) which has CysI ligating the unique $S = {}^5/_2$ Fe site and Asp at position II (*24*), and in *D. gigas* FdII (*22*) and *T. litoralis* Fd (*25*) which both have CysIV ligating the unique $S = {}^5/_2$ Fe site and Cys at position II. Since the $[Fe_3S_4]^+$ clusters in *D. gigas* FdII and *T. litoralis* Fd have EPR spectra identical to that of the D14C mutant of Pf Fd (*26*, *43*), we tentatively attribute type 1 and type 2 behavior to the more strongly coupled pair of Fe atoms being ligated by CysI/CysIII and CysIII/CysIV, respectively.

The difference between the two types of $[Fe_3S_4]^+$ clusters that is apparent in the ground state properties, as deduced from EPR, is not readily apparent in the excited state electronic structure as revealed by the VTMCD spectra (Figure 2). Indeed, the spectra of all seven $[Fe_3S_4]$ clusters are remarkably invariant to the nature of the residue at position II with only minor differences in the weak bands in the 600−800 nm region. While the VTMCD spectrum reveals the complexity of the excited state structure and is a useful fingerprint of cluster type (*44*), there are as yet no detailed assignments for the 16−18 S $\rightarrow$ Fe(III) charge transitions that are observed in the region of 280−800 nm.

The close correspondence in the RR spectra of these seven $[Fe_3S_4]^+$ clusters in the Fe−S stretching region (Figure 3) attests to very similar structures and cysteine Fe−S−C−C dihedral angles in each variant (*2*, *45*, *46*). The vibrational modes of the cuboidal $Fe_3S_4{}^bS_3{}^t$ unit (S^b being bridging or

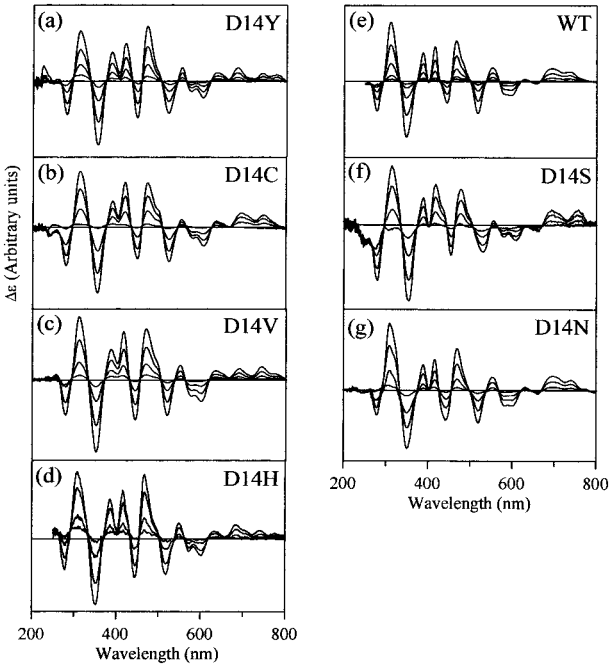

FIGURE 2: VTMCD spectra of $[Fe_3S_4]^+$ clusters in wild-type and mutant forms of *P. furiosus* Fd. All samples were in 100 mM Tris-HCl buffer (pH 7.8) with 55% (v/v) poly(ethylene glycol), and the MCD intensity at all wavelengths increases in intensity with decreasing temperature. (a) D14Y mutant, at 52 μM. MCD spectra recorded with a magnetic field of 4.5 T at 1.63, 4.22, 9.8, and 32.1 K. (b) D14C mutant, at 81 μM. MCD spectra recorded with a magnetic field of 6.0 T at 1.66, 4.22, 9.7, and 32.5 K. (c) D14V mutant, at 193 μM. MCD spectra recorded with a magnetic field of 4.5 T at 1.67, 4.22, 10.5, and 33.9 K. (d) D14H mutant, at 128 μM. MCD spectra recorded with a magnetic field of 4.5 T at 1.51, 4.22, 11.5, and 35.4 K. (e) Wild type, at 250 μM. MCD spectra recorded with a magnetic field of 4.5 T at 1.59, 4.22, 9.9, 17.6, and 53 K. (f) D14S mutant, at 169 μM. MCD spectra recorded with a magnetic field of 6.0 T at 1.64, 4.22, 9.7, and 32.6 K. (g) D14N mutant, at 229 μM. MCD spectra recorded with a magnetic field of 4.5 T at 1.69, 4.22, 10.5, and 33.5 K.

inorganic S and S^t being terminal or cysteinyl S) have been assigned under effective C_{3v} symmetry on the basis of normal mode calculations and $^{32/34}S^b$ and $^{54/56}Fe$ isotope shifts (*45*, *47*, *48*). The frequencies of the Fe−S stretching modes are essentially unperturbed in the mutant proteins, and the bands at 386 and 367 cm^{-1} are assigned primarily to the symmetric and asymmetric Fe−S^t stretching modes, respectively ($\leq$2 cm^{-1} $^{34}S^b$ downshifts), whereas the bands at 405, 397, 347, 290, and 265 cm^{-1} are assigned primarily to Fe−S^b stretching modes ($\geq$4 cm^{-1} $^{34}S^b$ downshifts). The most intense band at 347 cm^{-1} is assigned to the symmetric stretch of the Fe_3-(μ_3-S^b) unit, and the unresolved splitting in the asymmetric Fe−S^t stretching at 367 cm^{-1} reflects the lowering of symmetry from idealized C_{3v}. Close inspection of the spectra reveals that the two types of clusters distinguished by EPR are also differentiated in the RR spectra by the relative enhancements of the mainly terminal and bridging stretching modes at 386 and 397 cm^{-1}, respectively; type 2 generally has greater relative intensity at 386 cm^{-1}. However, the effect is subtle and suggests perturbation of the excited state properties rather than significant changes in the core structure.

Reduced $[Fe_3S_4]^0$ Clusters. Parallel-mode X-band EPR and VTMCD spectra for the $[Fe_3S_4]^0$ clusters in dithionite-reduced *P. furiosus* Fd with Asp, Cys, Ser, Val, His, Asn, and Tyr at position II are compared in Figures 4 and 5, respectively. Each sample exhibits a broad low-field resonance in the EPR spectrum that increases in intensity and sharpens in parallel mode compared to perpendicular mode (Figure 4). Such characteristics are the hallmark of an integer spin system, and by analogy with $[Fe_3S_4]^0$ clusters in other ferredoxins (*19*, *49*), this resonance is assigned to the transition within the $M_s = \pm 2$ doublet of an $S = 2$ ground state with the axial zero-field splitting parameter ($D < 0$). In a purely axial system, the effective principal *g*-values for this doublet are 8, 0, and 0. However, the observed low-field resonance is expected to increase above $g = 8$ with increasing rhombic distortion, since the zero-field splitting within the formal $M_s = \pm 2$ doublet corresponds to $3E^2/D$, where *E* is the rhombic zero-field splitting parameter (*19*, *50*). As shown in Figure 4, the effective *g*-value and breadth of this resonance for the $[Fe_3S_4]^0$ clusters in *P. furiosus* Fd are sensitive to the residue at position II, varying between 18.7 for D14Y and 11.9 for D14S (as estimated by the crossover point of the derivative). These differences reflect the magnitude and heterogeneity of *E*/*D*, but there does not

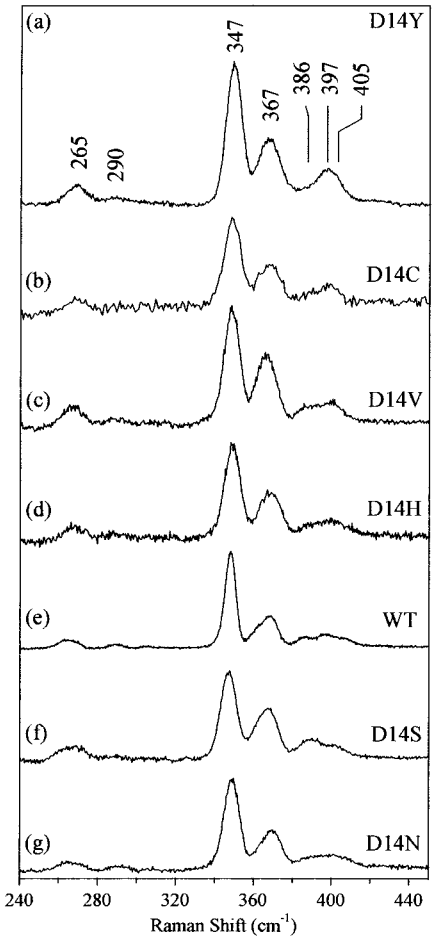

FIGURE 3: Resonance Raman spectra of $[Fe_3S_4]^+$ clusters in wild-type and mutant forms of *P. furiosus* Fd. All samples were approximately 2 mM in Fd and were in 100 mM Tris-HCl buffer (pH 7.8). Conditions of measurement were as follows: excitation wavelength, 457.9 nm; laser power at sample, 75 mW; sample temperature, 20 K; photon counting for 1 s every 0.4 cm^{-1} for each scan; and spectral resolution, 6 cm^{-1}. (a) D14Y mutant, with 36 scans. (b) D14C mutant, with 39 scans. (c) D14V mutant, with 40 scans. (d) D14H mutant, with 20 scans. (e) Wild type, with 18 scans. (f) D14S mutant, with 33 scans. (g) D14N mutant, with 37 scans.

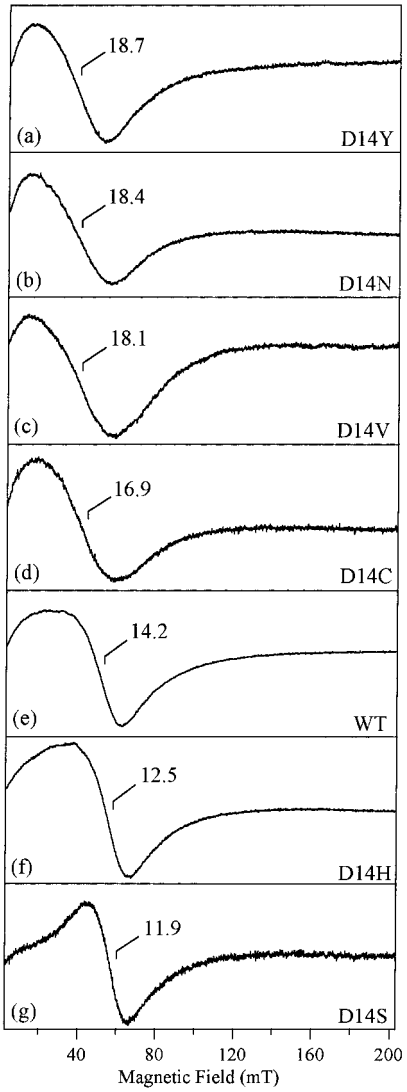

FIGURE 4: Parallel-mode X-band EPR spectra of $[Fe_3S_4]^0$ clusters in wild-type and mutant forms of dithionite-reduced *P. furiosus* Fd. The samples are the same as those used in Figure 1 and were anaerobically reduced with a 10-fold excess of dithionite. All spectra were recorded at 8.0 K under the following conditions: microwave power, 50 mW; microwave frequency, 9.37 GHz; and modulation amplitude, 0.63 mT. (a) D14Y mutant. (b) D14N mutant. (c) D14V mutant. (d) D14C mutant. (e) Wild type. (f) D14H mutant. (g) D14S mutant.

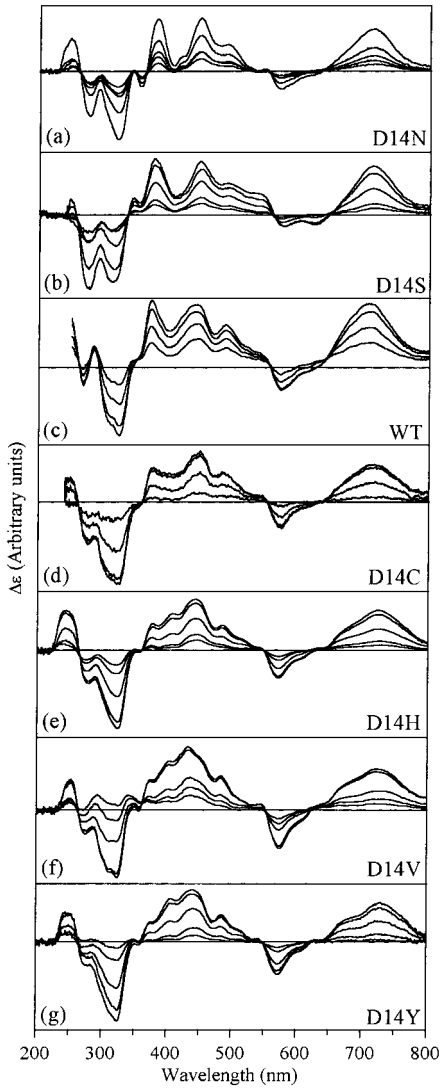

FIGURE 5: VTMCD spectra of $[Fe_3S_4]^0$ clusters in wild-type and mutant forms of dithionite-reduced *P. furiosus* Fd. All samples were in 100 mM Tris-HCl buffer (pH 7.8) with 55% (v/v) poly(ethylene glycol), and were reduced anaerobically with a 10-fold excess of dithionite. The MCD intensity at all wavelengths increases with decreasing temperature. (a) D14N mutant, at 150 μM. MCD spectra recorded with a magnetic field of 6.0 T at 1.54, 4.22, 11.6, 26.0, and 42.0 K. (b) D14S mutant, at 268 μM. MCD spectra recorded with a magnetic field of 4.5 T at 1.82, 4.22, 10.0, 23.5, and 44.4 K. (c) Wild type, at 250 μM. MCD spectra recorded with a magnetic field of 4.5 T at 1.64, 4.22, 10.0, and 18.5 K. (d) D14C mutant, at 132 μM. MCD spectra recorded with a magnetic field of 4.5 T at 1.69, 4.22, 9.30, and 43.5 K. (e) D14H mutant, at 78 μM. MCD spectra recorded with a magnetic field of 4.5 T at 1.78, 4.22, 9.9, 23.4, and 44.1 K. (f) D14V mutant, at 185 μM. MCD spectra recorded with a magnetic field of 6.0 T at 1.51, 4.22, 13.0, 26.0, and 45.3 K. (g) D14Y mutant, at 87 μM. MCD spectra recorded with a magnetic field of 4.5 T at 1.65, 4.22, 9.6, 23.6, and 42.8 K.

appear to be any obvious correlation between the trends in this parameter and the two distinct types of $[Fe_3S_4]^0$ centers that are clearly apparent in the VTMCD data (see below).

The nature of the residue at position II also has a pronounced influence on the excited state electronic structure of the $[Fe_3S_4]^0$ cluster in *P. furiosus* Fd as evidenced by the VTMCD spectra in the UV−visible region (Figure 5). On the basis of the VTMCD data for the $S = {}^9/_2$ valence-delocalized $[Fe_2S_2]^+$ clusters in *C. pasteurianum* 2Fe Fd (*31*, *32*), the visible and near-IR VTMCD spectra for $[Fe_3S_4]^0$ clusters are dominated by charge transfer and Fe−Fe transitions associated with the valence-delocalized pair. Hence, the observed differences are attributed to changes in the properties and/or location of the valence-delocalized pair. Moreover, more detailed analyses of the spectra indicate that each can be viewed as the sum of two distinct types with D14Y and D14N corresponding to almost homogeneous examples of type 1 and type 2, respectively. This is illustrated in Figure 6 which shows that the spectra observed in the D14H and D14C mutants are well simulated by adding different proportions of the D14Y and D14N spectra. This analysis suggests a direct correlation with the oxidized EPR data, with predominantly type 1 behavior being observed for D14Y, D14V, and D14C and predominantly type 2 behavior being observed for the wild type, D14N, and D14S. Hence, by analogy with the EPR analysis, we attribute the two distinct types of VTMCD spectra to different locations of

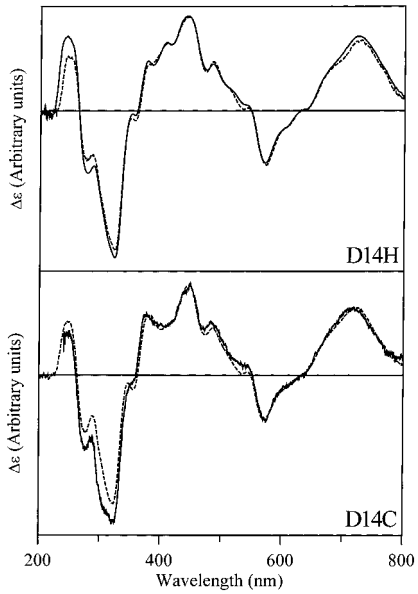

FIGURE 6: VTMCD spectra of the $[Fe_3S_4]^0$ clusters in D14H and D14C *P. furiosus* Fd simulated as the sum of the D14Y and D14N spectra: (top) 1.78 K MCD spectrum of the D14H mutant (solid line) (taken from Figure 5) and the sum of 0.82 × the D14Y 1.65 K MCD spectrum and 0.18 × the D14N 1.54 K MCD spectrum (broken line) and (bottom) 1.69 K MCD spectrum of the D14C mutant (solid line) (taken from Figure 5) and the sum of 0.55 × the D14Y 1.65 K MCD spectrum and 0.45 × the D14N 1.54 K spectrum (broken line).

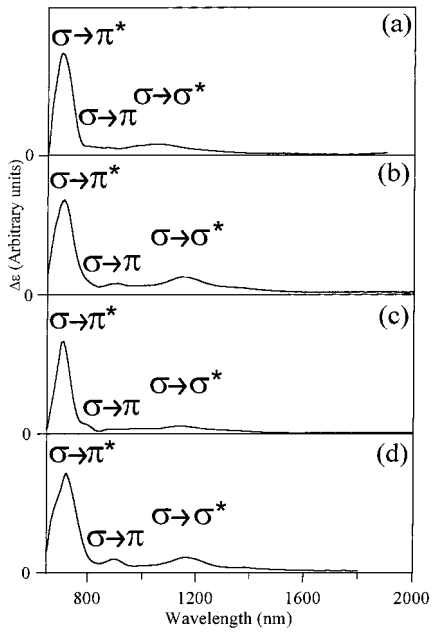

FIGURE 7: Comparison of the near-IR VTMCD spectrum of the $S = {}^9/_2$ valence-delocalized $[Fe_2S_2]^+$ cluster in the C60S mutant of *C. pasteurianum* 2Fe Fd (a) with those of the $[Fe_3S_4]^0$ clusters in wild-type (b), D14S (c), and D14V (d) *P. furiosus* Fd. The spectra were recorded at ~1.7 K with a magnetic field of 6 T. The samples were all approximately 300 μM in deuterated Tris-DCl buffer (pD 7.8) with 55% (v/v) deuterated ethylene glycol and were reduced anaerobically with a 10-fold excess of sodium dithionite.

the valence-delocalized pair. It is tempting to speculate that the pairwise intracluster Fe interactions are preserved on reduction; i.e., the more strongly coupled pair in the oxidized cluster accepts the electron to become the valence-delocalized pair on reduction. The only major discrepancy between the EPR and VTMCD categorizations is for the D14H variant which is predominantly type 2 in the reduced state as characterized by VTMCD, and type 1 in the oxidized state as characterized by EPR. This would require a change in the pairwise Fe interactions on reduction, and such a change also appears to occur to a smaller extent in the D14C mutant (55% type 1 and 45% type 2 on the basis of the VTMCD spectral simulation).

When the published VTMCD spectra for $[Fe_3S_4]^0$ clusters in different proteins are surveyed, it is particularly striking that each can be classified as predominantly type 1, e.g., *Desulfovibrio africanus* FdIII (*51*), *Solfolobus acidocaldarius* 7Fe Fd (high-pH, unprotonated form) (*52*), and spinach glutamate synthase (*53*), or predominantly type 2, e.g., *D. gigas* FdII (*27*), *P. furiosus* 3Fe Fd (*35*), *A. vinelandii* FdI (high-pH, unprotonated form) (*50*), *Azotobacter chroococcum* 7Fe Fd (high-pH form) (*54*), *Thermus thermophilus* 7Fe Fd (*50*), and aconitase (*55*). In other $[Fe_3S_4]$-containing enzymes, it is difficult to classify the spectral type due to interference from other paramagnetic clusters.

It is important to reemphasize that sequence specific assignments for the cysteine residues ligating a $[Fe_3S_4]^0$ cluster are not currently available in any protein. Despite numerous NMR studies of Fds containing $[Fe_3S_4]^0$ clusters (*22*, *24*, *25*, *56*−*61*), resonances from the β-CH_2 protons of the coordinating cysteines have yet to be assigned. The NMR line widths are considered to be too broad as a result of an abnormally long electronic relaxation time or exchange broadening. Since the extent of dipolar line broadening is much less for ^2H signals than for ^1H signals (due to the smaller magnetic moment of ^2H), the most recent attempt to use NMR to make sequence specific assignments of coordinating cysteine residues utilized the 7Fe Fd from *Bacillus schlegelii* in which the protein cysteines had been deuterated at the β position (*34*). While sharp ^2H NMR signals were observed for the cysteines ligating the $[Fe_3S_4]^+$ cluster, none were detected for the $[Fe_3S_4]^0$ cluster. Since theoretical considerations predict that these signals should be observable, it was concluded that the resonances coalesce due to the Fe sites exchanging valencies faster than the NMR time scale. This is consistent with the VTMCD data since in many cases two different pairwise arrangements appear to be "frozen-in" at low temperatures. Hence, at room temperature, it is likely that these conformations interchange faster than the NMR time scale.

The properties of the valence-delocalized pair in each of these two types of $[Fe_3S_4]^0$ clusters can be directly assessed by investigating the electronic transitions associated with the Fe−Fe interaction in the near-IR region. Near-IR VTMCD spectra of the wild type and D14S (representatives of type 2) and D14V (representative of type 1) are compared with that of the $S = {}^9/_2$ valence-delocalized $[Fe_2S_2]^+$ cluster in the C60S mutant of *C. pasteurianum* 2Fe Fd in Figure 7. The close correspondence in the spectra shows the presence of an $S = {}^9/_2$ valence-delocalized pair in each type of $[Fe_3S_4]^0$ cluster, and the transitions can be analyzed as described for the $[Fe_2S_2]^+$ cluster (*31*). A schematic molecular orbital diagram of the Fe−Fe interaction based on effective C_{2v} symmetry at the Fe sites is shown in Figure 8. The dominant interaction (responsible for the $S = {}^9/_2$ ground state) is the σ overlap between the pair of d_{z^2} orbitals, with progressively weaker π interactions, between pairs of d_{xz} and d_{yz} orbitals,

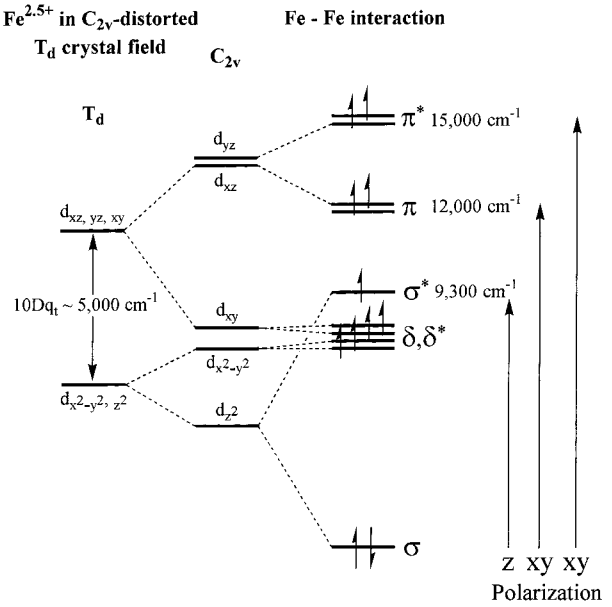

FIGURE 8: Schematic MO diagram for the Fe−Fe interaction in a valence-delocalized $S = {}^9/_2$ $[Fe_2S_2]^+$ unit. Modified from ref *31*.

and δ interactions, between pairs of d_{xy} and $d_{x^2-y^2}$ orbitals. The three highest-energy transitions are predicted to be $\sigma \rightarrow \sigma^*$ (electric dipole-allowed, but *z*-polarized resulting in weak VTMCD intensity), $\sigma \rightarrow \pi$ (*xy*-polarized, but electric dipole-forbidden resulting in weak VTMCD intensity), and $\sigma \rightarrow \pi^*$ (*xy*-polarized and electric dipole-allowed resulting in strong VTMCD intensity). The latter two transitions are expected to be derivative-shaped (pseudo *A* terms) and are likely to be split in low-symmetry biological environments. The assignments of these three transitions for the $S = {}^9/_2$ valence-delocalized $[Fe_2S_2]^+$ cluster in the C60S mutant of *C. pasteurianum* 2Fe Fd are shown in Figure 8. The energy of the *z*-polarized $\sigma \rightarrow \sigma^*$ transition is particularly important since it corresponds to 2β (or $10B$), where β is the resonance energy and *B* is the double exchange parameter.

To confirm analogous assignments for $[Fe_3S_4]^0$ clusters and hence quantify the resonance energy for the $S = {}^9/_2$ valence-delocalized pairs in each of the two distinct types, MCD magnetization data for the D14S sample were collected at 713 and 1148 nm (Figure 9). Uniaxial transitions such as the $\sigma \rightarrow \sigma^*$ transition of an Fe−Fe interaction are predicted to have anomalous MCD magnetization properties for transitions originating from a highly anisotropic doublet (*50*, *62*). This situation pertains to reduced $[Fe_3S_4]^0$ clusters, since the transitions arise from the $M_s = \pm 2$ doublet of the $S = 2$ manifold, which has a $g_{||}$ of 8.0 and a $g_\perp$ of 0.0 in the limit of a completely axial zero-field splitting. Completely different MCD magnetization data are observed for the bands centered at 713 and 1148 nm. The lowest temperature data at 713 nm are well fit by theoretical data constructed for a *xy*-polarized transition arising from a doublet with a $g_{||}$ of 8.0 and a $g_\perp$ of 0.0 (*62*). In contrast, the anomalous magnetization behavior at 1148 nm, i.e., increasing to a maximum and then decreasing as a function of $\beta B/2kT$, is predicted only for a predominantly *z*-polarized transition, when both the *z*-polarized and *xy*-polarized transition dipole moments (m_z and m_{xy}, respectively) have the same sign (*62*). For example, the lowest temperature data at 1148 nm is fit by a theoretical curve constructed from a *z*-polarized transition ($m_z/m_{xy} = 55$) with a $g_{||}$ of 8.0 and a $g_\perp$ of 0.1. The lowest-energy near-IR VTMCD band in each of the $[Fe_3S_4]^0$ spectra, therefore, corresponds to the uniaxial $\sigma \rightarrow \sigma^*$ transition of Fe−Fe interaction, and the resonance delocalization energy, β, is determined to be $4290 \pm 25\ cm^{-1}$ for type 1 clusters and $4350 \pm 25\ cm^{-1}$ for type 2 clusters. We conclude that the Fe−Fe interactions within the valence-delocalized pair are very similar in both locations.

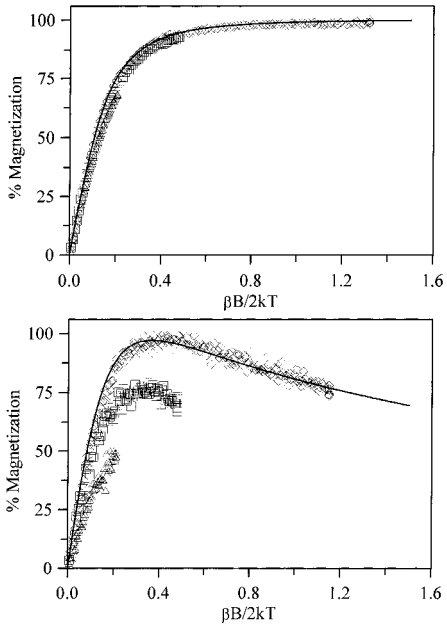

FIGURE 9: MCD magnetization data for the $[Fe_3S_4]^0$ cluster in the D14S mutant of dithionite-reduced *P. furiosus* Fd. The sample is described in the legend of Figure 7. (Top) Magnetization data collected at 713 nm, with magnetic fields between 0 and 6.0 T at (◇) 1.68, (□) 4.22, and (△) 9.7 K. The solid line depicts the theoretical magnetization data constructed for an *xy*-polarized transition originating from the $M_s = \pm 2$ doublet of an axial $S = 2$ ground state, with a $g_{||}$ of 8.0 and a $g_\perp$ of 0.0 (*62*). (Bottom) Magnetization data collected at 1148 nm, with magnetic fields between 0 and 6.0 T at (◇) 1.75, (□) 4.22, and (△) 9.62 K. The solid line depicts the theoretical magnetization data constructed for a predominantly *z*-polarized transition originating from the $M_s = \pm 2$ doublet of an $S = 2$ ground state, with a $g_{||}$ of 8.0 and a $g_\perp$ of 0.1, and an m_z/m_{xy} of 55 (*62*).

Rationalizing the Redox Potentials of $[Fe_3S_4]^{+,0}$ Clusters. The redox potential of the $[Fe_3S_4]^{+,0}$ couple in *P. furiosus* Fd was found to be very dependent on the nature on the residue at position II; E_m (pH 7 vs NHE) = −203, −188, −148, −129, −125, and −89 mV for the wild type, D14V, D14Y, D14H, D14N, and D14S, respectively (*36*). On the basis of the data presented herein, it is tempting to conclude that the location of the reducible pair is a major factor in determining the redox potential, since the mutants with type 2 arrangements (D14N and D14S) generally have significantly higher reduction potentials than type 1 arrangements (D14V and D14Y). However, the observation that the wild type (type 2) has the lowest potential is clearly contrary to this argument and demonstrates that other factors such as solvent exposure and changes in hydrogen bonding interactions that contribute to the electrostatic potential at the cluster are likely to be equally important. Molecular mechanics and dynamics calculations studies are planned to address the dependence of the redox potential on the nature of the residue at position II.

CONCLUSIONS

The three major conclusions of this work are summarized below.

(1) The results presented herein provide the first evidence that EPR and VTMCD are capable of assessing the pairwise Fe interactions of the oxidized and reduced $[Fe_3S_4]^{+,0}$ clusters, respectively. Although the specific assignments for these mutants of *P. furiosus* Fd require confirmation via NMR studies, the available NMR data for 3Fe Fds suggest two distinct arrangements: type 1 with CysIV ligating the unique Fe site and CysI and CysIII ligating the reducible pair and type 2 with CysI ligating the unique Fe site and CysIII and CysIV ligating the reducible pair.

(2) The nature of the residue at position II is a key determinant of the specific pairwise Fe interactions within $[Fe_3S_4]^{+,0}$ clusters in Fds with the type 1 arrangement favored by Tyr, Val, and Cys and the type 2 arrangement favored by Asp, Asn, and Ser. With His at position II, the pairwise arrangement changes from type 2 to predominantly type 1 on reduction. Partial type 1 to type 2 conversion occurs with Cys in position II on reduction. The D14Y and D14N mutants are almost exclusively type 1 and type 2, respectively, in the reduced form at cryogenic temperatures. Consequently, these mutants are the best candidates for NMR studies for assigning the cysteines ligating the specific Fe sites of a $[Fe_3S_4]^0$ cluster.

(3) Near-IR VTMCD provides a method for determining the resonance delocalization energy associated with the Fe−Fe interaction of the $S = {}^9/_2$ valence-delocalized pair in $[Fe_3S_4]^0$ clusters. The results for type 1 and type 2 $[Fe_3S_4]^0$ clusters indicate that the resonance energy is $\sim$4300 cm^{-1} and relatively independent of the specific location of the valence-delocalized pair.

REFERENCES

1. Emptage, M. H., Kent, T. A., Huynh, B. H., Rawlings, J., Orme-Johnson, W. H., and Münck, E. (1980) *J. Biol. Chem. 255*, 1793−1796.
2. Johnson, M. K., Duderstadt, R. E., and Duin, E. C. (1999) *Adv. Inorg. Chem. 47*, 1−82.
3. Beinert, H., and Thomson, A. J. (1983) *Arch. Biochem. Biophys. 222*, 333−361.
4. Matsubara, H., and Saeki, K. (1992) *Adv. Inorg. Chem. 38*, 223−280.
5. Stout, G. H., Turley, S., Sieker, L. C., and Jensen, L. H. (1988) *Proc. Natl. Acad. Sci. U.S.A. 85*, 1020−1022.
6. Stout, C. D. (1989) *J. Mol. Biol. 205*, 545−555.
7. Stout, C. D., Stura, E. A., and McRee, D. E. (1998) *J. Mol. Biol. 278*, 629−639.
8. Kissinger, C. R., Adman, E. T., Sieker, L. C., and Jensen, L. H. (1988) *J. Am. Chem. Soc. 110*, 8721−8723.
9. Kissinger, C. R., Sieker, L. C., Adman, E. T., and Jensen, L. H. (1991) *J. Mol. Biol. 219*, 693−715.
10. Robbins, A. H., and Stout, C. D. (1985) *J. Biol. Chem. 260*, 2328−2333.
11. Robbins, A. H., and Stout, C. D. (1989) *Proteins 5*, 289−312.
12. Volbeda, A., Charon, M.-H., Piras, C., Hatchikian, E. C., Frey, M., and Fontecilla-Camps, J. C. (1995) *Nature 373*, 580−587.
13. Higuchi, Y., Yagi, T., and Yasuoka, N. (1997) *Structure 5*, 1671−1680.
14. Fujii, T., Hata, Y., Oozeki, M., Moriyama, H., Wakagi, T., Tanaka, H., and Oshima, T. (1997) *Biochemistry 36*, 1505−1513.
15. Stout, C. D. (1993) *J. Biol. Chem. 268*, 25920−25927.
16. Zhou, J., Hu, Z., Münck, E., and Holm, R. H. (1996) *J. Am. Chem. Soc. 118*, 1966−1980.
17. Kent, T. A., Huynh, B. H., and Münck, E. (1980) *Proc. Natl. Acad. Sci. U.S.A. 77*, 6574−6576.
18. Münck, E., and Kent, T. A. (1986) *Hyperfine Interact. 27*, 161−172.
19. Papaefthymiou, V., Girerd, J.-J., Moura, I., Moura, J. J. G., and Münck, E. (1987) *J. Am. Chem. Soc. 109*, 4703−4710.
20. Gayda, J.-P., Bertrand, P., Theodule, F.-X., and Moura, J. J. G. (1982) *J. Chem. Phys. 77*, 3387−3391.
21. Day, E. P., Peterson, J., Bonvoisin, J. J., Moura, I., and Moura, J. J. G. (1988) *J. Biol. Chem. 263*, 3684−3689.
22. Macedo, A. L., Moura, I., Moura, J. J. G., LeGall, J., and Huynh, B. H. (1993) *Inorg. Chem. 32*, 1101−1105.
23. Yoo, S. J., Hu, Z., Goh, C., Bominaar, E. L., Holm, R. H., and Münck, E. (1997) *J. Am. Chem. Soc. 119*, 8732−8733.
24. Gorst, C. M., Yeh, Y.-H., Teng, Q., Calzolai, L., Zhou, Z.-H., Adams, M. W. W., and La Mar, G. N. (1995) *Biochemistry 34*, 600−611.
25. Donaire, A., Gorst, C. M., Zhou, Z.-H., Adams, M. W. W., and La Mar, G. N. (1994) *J. Am. Chem. Soc. 116*, 6841−6849.
26. Huynh, B. H., Moura, J. J. G., Moura, I., Kent, T. A., LeGall, J., Xavier, A. V., and Münck, E. (1980) *J. Biol. Chem. 255*, 3242−3244.
27. Thomson, A. J., Robinson, A. E., Johnson, M. K., Moura, J. J. G., Moura, I., Xavier, A. V., and LeGall, J. (1981) *Biochim. Biophys. Acta 670*, 93−100.
28. Girerd, J.-J. (1983) *J. Chem. Phys. 79*, 1766−1775.
29. Borshch, S. A., Bominaar, E. L., Blondin, G., and Girerd, J.-J. (1993) *J. Am. Chem. Soc. 115*, 5155−5168.
30. Beinert, H., Holm, R. H., and Münck, E. (1997) *Science 277*, 653−659.
31. Johnson, M. K., Duin, E. C., Crouse, B. R., Golinelli, M.-P., and Meyer, J. (1998) in *Spectroscopic Methods in Bioinorganic Chemistry* (Solomon, E. I., and Hodgson, K. O., Eds.) pp 286−301, American Chemical Society, Washington, DC.
32. Crouse, B. R., Meyer, J., and Johnson, M. K. (1995) *J. Am. Chem. Soc. 117*, 9612−9613.
33. Achim, C., Golinelli, M.-P., Bominaar, E. L., Meyer, J., and Münck, E. (1996) *J. Am. Chem. Soc. 118*, 8168−8169.
34. Bertini, I., Luchinat, C., Mincione, G., and Soriano, A. (1998) *Inorg. Chem. 37*, 969−972.
35. Conover, R. C., Kowal, A. T., Fu, W., Park, J.-B., Aono, S., Adams, M. W. W., and Johnson, M. K. (1990) *J. Biol. Chem. 265*, 8533−8541.
36. Brereton, P. S., Verhagen, M. F. J. M., Zhou, Z.-H., and Adams, M. W. W. (1998) *Biochemistry 37*, 7351−7362.
37. Frauenfelder, H., Sligar, S. G., and Wolynes, P. G. (1991) *Science 254*, 1598−1603.
38. Fan, C., Houseman, A. L. P., Doan, P. E., and Hoffman, B. M. (1993) *J. Phys. Chem. 97*, 3017−3021.
39. Guigliarelli, B., Gayda, J.-P., Bertrand, P., and More, C. (1986) *Biochim. Biophys. Acta 871*, 149−155.
40. Guigliarelli, B., More, C., Bertrand, P., and Gayda, J.-P. (1986) *J. Chem. Phys. 85*, 2774−2778.
41. Hagen, W. R. (1992) *Adv. Inorg. Chem. 38*, 165−222.
42. Telser, J., Huang, H., Lee, H.-I., Adams, M. W. W., and Hoffman, B. M. (1998) *J. Am. Chem. Soc. 120*, 861−870.
43. Hankins, H. L. (1994) M.S. Dissertation, University of Georgia, Athens, GA.
44. Johnson, M. K., Robinson, A. E., and Thomson, A. J. (1982) in *Iron−Sulfur Proteins* (Spiro, T. G., Ed.) pp 367−406, Wiley-Interscience, New York.
45. Johnson, M. K., Czernuszewicz, R. S., Spiro, T. G., Fee, J. A., and Sweeney, W. V. (1983) *J. Am. Chem. Soc. 105*, 6671−6678.
46. Spiro, T. G., Czernuszewicz, R. S., and Han, S. (1988) in *Resonance Raman Spectra of Heme and Metalloproteins* (Spiro, T. G., Ed.) pp 523−554, John Wiley & Sons, New York.
47. Fu, W. (1990) M.S. Dissertation, University of Georgia, Athens, GA.

48. Kilpatrick, L. K., Kennedy, M. C., Beinert, H., Czernuszewicz, R. S., Qui, D., and Spiro, T. G. (1994) *J. Am. Chem. Soc. 116*, 4053−4060.
49. Hagen, W. R., Dunham, W. R., Johnson, M. K., and Fee, J. A. (1985) *Biochim. Biophys. Acta 828*, 369−374.
50. Johnson, M. K., Bennett, D. E., Fee, J. A., and Sweeney, W. V. (1987) *Biochim. Biophys. Acta 911*, 81−94.
51. Armstrong, F. A., George, S. J., Cammack, R., Hatchikian, E. C., and Thomson, A. J. (1989) *Biochem. J. 264*, 265−273.
52. Breton, J. L., Duff, J. L. C., Butt, J. N., Armstrong, F. A., George, S. J., Petillot, Y., Forest, E., Schafer, G., and Thomson, A. J. (1995) *Eur. J. Biochem. 233*, 937−946.
53. Knaff, D. B., Hirasawa, M., Ameyibor, E., Fu, W., and Johnson, M. K. (1991) *J. Biol. Chem. 266*, 15080−15084.
54. George, S. J., Richards, A. J. M., Thomson, A. J., and Yates, M. G. (1984) *Biochem. J. 224*, 247−251.
55. Johnson, M. K., Thomson, A. J., Richards, A. J. M., Peterson, J., Robinson, A. E., Ramsay, R. R., and Singer, T. P. (1984) *J. Biol. Chem. 259*, 2274−2282.
56. Cheng, H., Grohmann, K., and Sweeney, W. V. (1992) *J. Biol. Chem. 267*, 8073−8080.
57. Nagayama, K., Ohmori, D., Imai, T., and Oshima, T. (1983) *FEBS Lett. 158*, 208−212.
58. Busse, S. C., La Mar, G. N., Yu, L. P., Howard, J. B., Smith, E. T., Zhou, Z.-H., and Adams, M. W. W. (1992) *Biochemistry 31*, 11952−11962.
59. Bentrop, D., Bertini, I., Luchinat, C., Mendes, J., Piccioli, M., and Teixeira, M. (1996) *Eur. J. Biochem. 236*, 92−99.
60. Aono, S., Bertini, I., Cowan, J. A., Luchinat, C., Rosato, A., and Viezzoli, M. S. (1996) *JBIC, J. Biol. Inorg. Chem. 1*, 523−528.
61. Bertini, I., Dikiy, A., Luchinat, C., Macinai, R., Viezzoli, M. S., and Vincenzini, M. (1997) *Biochemistry 36*, 3570−3579.
62. Bennett, D. E., and Johnson, M. K. (1987) *Biochim. Biophys. Acta 911*, 71−80.

BI990670L